MAGNETIC BUBBLE MATERIALS

Monsanto Research Corporation
St. Louis, Missouri 63166

INITIAL CHARACTERIZATION REPORT

March 1972

Contract No. DAAH01-72-C-0490

Distribution of this document is unlimited

ARPA Support Office
Research, Development, Engineering,
and Missile Systems Laboratory
U.S. Army Missile Command
Redstone Arsenal, Alabama

Sponsored by:
Advanced Research Projects Agency
ARPA Order Nr. 1999

NOTICE

This research was sponsored by the Advanced Research Projects Agency of the Department of Defense under ARPA Order 1999 and was monitored by the US Army Missile Command under Contract Number DAAH01-72-C-0490. Views and conclusions expressed herein are the primary responsibility of the author or the contractor and should not be interpreted as representing the official opinion or policy of USAMICOM, ARPA, DOD or any other agency of the Government.

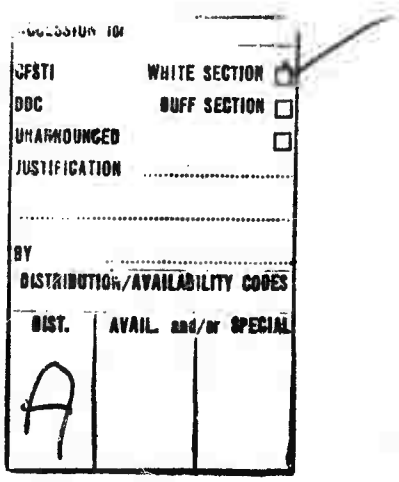

UNCLASSIFIED
Security Classification

DOCUMENT CONTROL DATA · R & D

(Security classification of title, body of abstract and indexing annotation must be entered when the overall report is classified)

1. ORIGINATING ACTIVITY *(Corporate author)*
Monsanto Research Corporation
800 North Lindbergh Boulevard
St. Louis, Missouri 63166

2a. REPORT SECURITY CLASSIFICATION
UNCLASSIFIED

2b. GROUP

3. REPORT TITLE
MAGNETIC BUBBLE MATERIALS

4. DESCRIPTIVE NOTES *(Type of report and inclusive dates)*
INITIAL CHARACTERIZATION REPORT

5. AUTHOR(S) *(First name, middle initial, last name)*
Jerry W. Moody
Robert M. Sandfort
Roger W. Shaw

6. REPORT DATE
March 1972

7a. TOTAL NO. OF PAGES
49

7b. NO. OF REFS
25

8a. CONTRACT OR GRANT NO.
DAAH01-72-C-0490

b. PROJECT NO.
ARPA Order No. 1999-72

c.

d.

9a. ORIGINATOR'S REPORT NUMBER(S)

9b. OTHER REPORT NO(S) *(Any other numbers that may be assigned this report)*

10. DISTRIBUTION STATEMENT
Distribution of this document unlimited

11. SUPPLEMENTARY NOTES

12. SPONSORING MILITARY ACTIVITY
Advanced Research Projects Agency
Washington, D.C.

13. ABSTRACT

This report discusses methods used by Monsanto Research Corporation for the characterization of magnetic bubble materials in the initial phase of Contract No. DAAH01-72-C-0490. These materials are magnetic garnet films epitaxially deposited on non-magnetic garnet substrates. Properties included in the garnet characterization and in this report are the following: for substrates - defect identification; for substrates and films - composition and lattice parameters; for films only - thickness and thickness variation, defect detection and location, characteristic length and domain dimensions, saturation magnetization and magnetic field, anisotropy field, coercivity, domain wall mobility, and Neel temperature. Emphasis is on experimental detail with theory covered by appropriate references where possible.

DD FORM 1 NOV 65 1473

UNCLASSIFIED
Security Classification

14. KEY WORDS	LINK A		LINK B		LINK C	
	ROLE	WT	ROLE	WT	ROLE	WT
Single Crystal Rare Earth Garnets						
Characterization Methods for Bubble Garnets						
Magnetic Domains						
Memory Devices						

TECHNICAL REQUIREMENT NO. 1533
ARPA ORDER 1999

MAGNETIC BUBBLE MATERIALS

INITIAL CHARACTERIZATION REPORT

March 1972

MONSANTO RESEARCH
CORPORATION
St. Louis, Missouri 63166
Contract No. DAAH01-72-C-0490

Monitored By
ARPA Support Office
Research, Development, Engineering, and
Missile Systems Laboratory

Sponsored by:
Advanced Research Projects Agency
Washington, D.C., ARPA Order Nr. 1999

ABSTRACT

This report discusses methods used by Monsanto Research Corporation for the characterization of magnetic bubble materials in the initial phase of Contract No. DAAH01-72-C-0490. These materials are magnetic garnet films epitaxially deposited on non-magnetic garnet substrates. Properties included in the garnet characterization and in this report are the following: for substrates - defect identification; for substrates and films - composition and lattice parameter; for films only - thickness and thickness variation, defect detection and location, characteristic length and domain dimensions, saturation magnetization and magnetic field , anisotropy field, coercivity, domain wall mobility, and Neel temperature. Emphasis is on experimental detail with theory covered by appropriate references where possible.

Table of Contents

List of Figures

List of Tables

I. Introduction

The concepts and materials which will be put to use in magnetic bubble devices are undergoing an extremely rapid evolution. Keeping pace with this evolution, older magnetic material measurement methods are being adapted to the special requirements of these thin, transparent films. In addition new methods of measurement are being developed which take advantage of the unique properties of these films, in particular the easily observed Faraday effect in the visible portion of the electromagnetic spectrum. There is no doubt that further refinements will take place in the methods and the properties used to characterize these materials. Improved accuracy, more reliable prediction of device performance, and more rapid data acquisition and analysis are all desirable and will be achieved.

This contract requires the conduct of a study of the state of the art in the characterization of single-crystal, non-magnetic substrates and single-crystal thin magnetic films, including establishment of all the items required to be characterized, determination of the known techniques for each of the methods of characterization and identification of the recommended characterization method for each item. As an interim measure, this report establishes an initial list of items characterized and the method used for characterization of materials now being supplied under this contract. Accordingly, this report does not cover all items requiring characterization. Certain items now being characterized by others are not presented in this report since they are not now being used in this contract.

The methods employed at Monsanto Research Corp. for the characterization of magnetic bubble materials supplied to the Advanced Research Projects Agency under contract No. DAAH01-72-C-0490 are presented in detail. The emphasis of the report is on experimental detail, with a minimum of theoretical development. If a more detailed theoretical treatment is desired, the reader is directed in each case to the pertinent literature references. It is the authors' hope that this emphasis will aid the reader in evaluating the techniques employed and implementing them, if desired, with a minimum of difficulty. The methods used to measure the following properties are discussed:

Composition

Lattice parameter

Substrate defects

Thickness

Thickness variation

Defects

Defect location

ℓ - characteristic length

$4 \pi M_s$

H_A - anisotropy field

H_C - coercivity

μ_w - wall mobility

T_N - Neel temperature

Bubble diameters

Bias fields

II. Composition

Electron Probe Microanalysis (EPM) has been utilized to characterize the composition of the magnetic garnet epitaxial layers. The concentrations of all elements composing the garnet matrix have been determined quantitatively with the exception of oxygen. The concentration of oxygen in all determinations has been assumed to compose the balance of the composition. This is necessary since the instrument used for the analysis does not have the capability to detect elements lighter than aluminum.

The reasons for employing EPM to determine the composition of these materials are three fold:

1) The effective volume of characteristic X-ray production for this particular instrument is approximately 2 μm^3. This shallow penetration of the epitaxial layer insures that only the area of interest is considered in the determination.

2) Due to the small area of analysis, it is possible to perform homogeniety determinations over the surface of the epitaxial layer.

3) Since the technique is non destructive it is possible to utilize the film in further testing and evaluation subsequent to EPM analysis.

For the EuEr samples evaluated to date, the concentration of rare earth metals, lead, and iron have been determined by comparison to pure metal forms of these elements. The determination of gallium concentration was made by comparison to gallium phosphide. The purity of the standards used is as follows:

Rare earths - 99.9%

Fe - Spectrographic grade

Pb - Spectrographic - grade

GaP - Monsanto Semiconductor

Matrix corrections are applied when the sample counts are compared to the standards. The accuracy of the method is approximately 3% of the actual concentration of the metals.

Since the electron beam samples an area only about 2 microns in diameter, the compositional uniformity of the epitaxial layers is determined by taking counts at a number of widely separated points on each layer. The agreement of these determinations is, in general, well within the experimental accuracy of the method. The compositional uniformity of the layers is also checked by measuring the Neel temperature at various points. This measurement is discussed in section XIII. Again, the results at various points on a given sample generally agree within the accuracy of the method.

III. Lattice Parameter

The room temperature lattice parameter mismatch between the magnetic garnet film and the non-magnetic garnet substrate determines the state of stress existing in the film (Ref. 1). Since the film stress contributes to the uniaxial anisotropy through the magnetostriction coefficients, it is important to know the film and the substrate lattice constants. Both are measured simultaneously by a single crystal X-ray diffraction technique (Ref. 2). The samples are irradiated with $K\alpha$ and $K\alpha_2$ molybdenum x-ray radiation, and the angular location, 2θ, of the diffraction peaks from the (888), (12 12 12), and (16 16 16) planes are recorded on a strip chart recorder. The d-spacings are obtained from tables and are then converted to lattice parameters. The lattice parameters obtained from the d-spacings are plotted versus $\cot^2 \theta$ where θ is one-half the angular location of the diffraction peak. This line extrapolated to $\cot^2 \theta = 0$ yields the lattice parameter. When film and substrate lattice parameters are different, two distinct peaks are obtained for the same wavelength radiation, one corresponding to the film and one to the substrate. This simultaneous measurement is made only occasionally, while the substrate lattice constant is routinely measured in the absence of an epitaxial film. The lattice constant measurement is accurate to ± 0.0001Å.

IV. Substrate Defect Identification

Many of the defects which impede the motion of magnetic domains in the epitaxial films have their origin in the substrate. These include dislocations, growth striations, strain, inclusions, scratches and work damage resulting from improper lapping and polishing procedures. Most of these defects can be discovered by microscopic examination of the polished or etched substrates.

Inclusions of a foreign phase most often result from stoichiometric deviations or from the incorporation of metallic iridium particles in the growing crystal. These defects are readily seen under the microscope in ordinary transmitted light.

The "core" region of a garnet boule is a highly strained region found near the center of the crystal. It results from the formation of (211) or (110) facets at the solid-liquid interface during crystal growth. Although the "core" is a common defect of garnets grown by the Czochralski method, it can be eliminated by adjusting the growth conditions. The "core" region and other strains are studied with the aid of a polarizing microscope. The presence of strain induces birefringence in the crystal which manifests itself as color and intensity variation when observed in transmitted, polarized light In the same way, polarized light is useful in detecting the strain associated with inclusions which might not be easily seen with ordinary transmitted light. (Ref. 3)

Dislocations in garnets can be selectively etched in orthophosphoric acid at 160 - 170°C. This treatment also reveals the presence of growth striations. (The origin of growth striations in garnets is not well understood but is believed to be associated with small stoichiometric deviations.) Both of these defects are best assessed with a phase interference microscope. Scratches or other residual work damage can also be found using this instrument. (Ref. 4)

V. Film Thickness

The thickness of the bubble film is central to the evaluation of several important magnetic properties, including the stable domain range and the saturation magnetization. The method used to measure this thickness is optical reflectivity in the red and infrared range of wavelengths: 0.6 to 1.0 microns. The optical index of refraction of the non-magnetic garnet substrate material is sufficiently different from the magnetic-bubble film that significant reflection of light occurs at that interface. When this reflected light passes out through the front surface once again and recombines with light reflected from the front surface, optical interference between these two beams occurs. If monochromatic light of wavelength λ is employed, the reflected light intensity will then be found to oscillate as λ is varied. A typical curve of this type is shown in Figure 1b. From such data the thickness may be calculated as:

$$h = \left[2n \left(\frac{1}{\lambda_{m+1}} - \frac{1}{\lambda_m} \right) \right]^{-1}$$

Here n is the index of refraction of the magnetic film and λ_{m+1} and λ_m are wavelengths corresponding to successive maxima or minima in the reflectivity. In practice the average spacing in $\frac{1}{\lambda}$ for a large number of oscillations is used at Monsanto in order to improve accuracy. Typically the wavelength range 0.60 to 1.0 μm is used because of the convenience of silicon solar cell detectors. In this range the index of refraction is taken as n = 2.35 in accordance with the results of Roman, Spiwak, and Baron of Bell Telephone Laboratories. (Ref. 5)

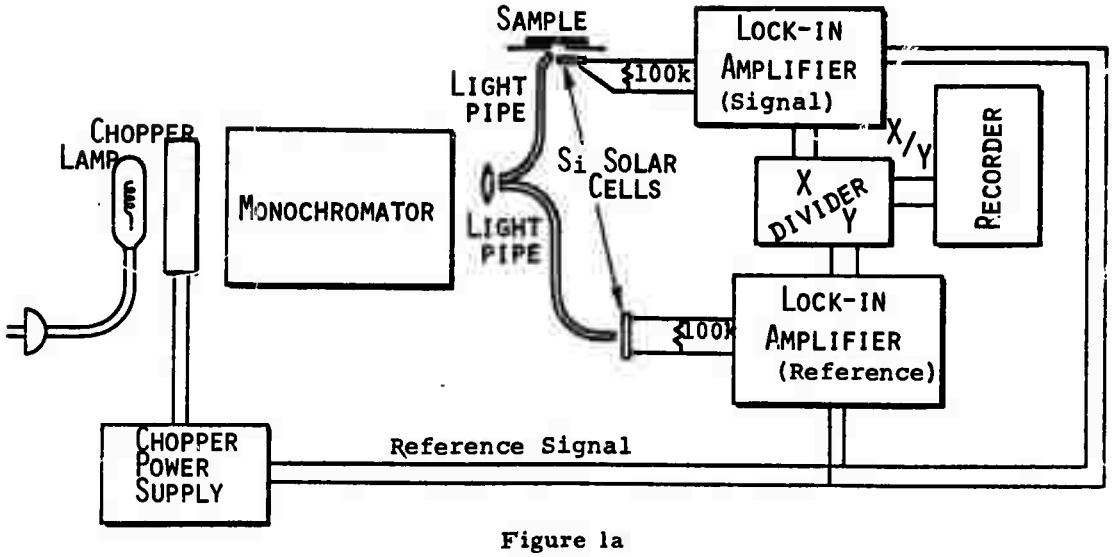

Figure 1a

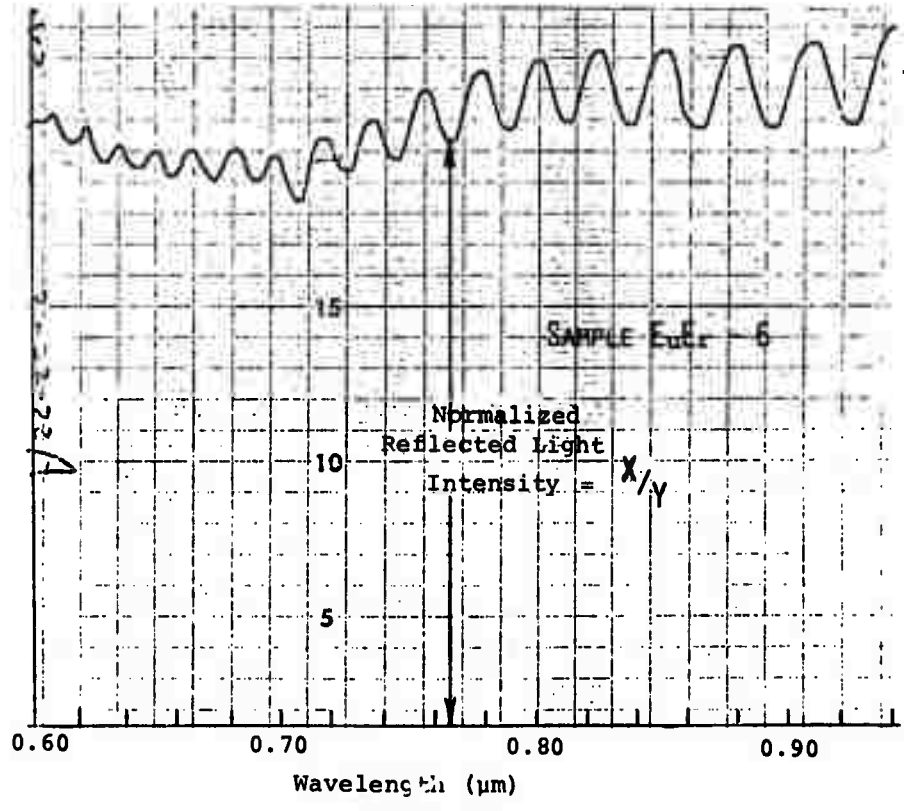

Figure 1b

Figure 1. Thickness System

Any spectrometer with visible-near infrared capabilities and reflectivity attachment can be used for this measurement. For completeness, however, we show the specific system being used at Monsanto in Figure 1a. Both the monochromator and recorder have time drives, the rates of which are chosen in conjunction with the monochromator slit widths and lock-in amplifier time constants to yield reliable data. For a chart such as Fig 1b the following settings prevail: Monochromator resolution - 14Å, scan rate - 2 Å/sec. lock-in amplifier time constant - 1 sec. so that the complete scan shown required 28 minutes. With only minor reduction in signal to noise a time constant of 0.3 sec and scan rate of 5 Å/sec can be used yielding an acquisition time of 11 min. Further reductions in acquisition time are definitely possible. The monochromator is provided with a marker circuit which provides output pulses at fixed wavelengths and which are duly recorded by an event marker on the recorder. The purpose of the reference channel detector, lock-in amplifier and divider unit is to cancel variations in light intensity with wavelength and time. The size of the aperture through which light is incident on the sample is 1 x 2 mm.

Known sources of uncertainty in this measurement are 1) variation of n with wavelength over the range employed ± 3%; 2) uncertainty in n at fixed wavelength (including differences between various film compositions) ±2%; 3) uncertainty in the determination of $\lambda_{m+1}^{-1} - \lambda_{m}^{-1}$ ± 2%. Combining these uncertainties leads to a range of probable error in the resulting thickness of approximately ± 4%. This figure represents the accuracy with which the thickness is known at the spot on the sample at which the reflectivity was observed. Variations in thickness over the sample area are separately handled by means of the thickness map.

VI. Thickness Variations

Interference effects entirely similar to those described in section V when wavelength is varied would also be observed if the film thickness were varied at constant wavelength. Such an effect is actually observed when regions of different thickness are present in the same sample. In this case the dark bands arising from destructive interference in the reflected light correspond to contours of constant film thickness satisfying the relationship $2 h n = m \lambda$. Here h is the film thickness, n, the index of refraction at wavelength λ, and m, an integer. The difference in thickness between successive dark bands is then $\Delta h = \lambda / 2n$. We are using a helium filled discharge lamp which provides a strong line at 0.5876 μm wavelength. This yields a thickness difference between the successive dark bands of (0.122 ± 0.005) μm based upon $n = 2.40$ at this wavelength. These bands are readily visible to the eye when viewed in this light. This technique has proved invaluable in our efforts to improve film flatness. In order to photograph the interference fringes a glass beam splitter is used as indicated in Fig. 2a . A typical result is shown in Fig. 2b

Such a map in itself does not show the sign of the thickness gradient. This can often be determined by visual inspection since a significantly thicker region will appear darker green. If the thickness variations are so small to yield detectable color differences another simple technique is still available. This involves rotating the sample while viewing the fringes under monochromatic light. As the sample is rotated away from a perpendicular viewing angle the dark bands appear to move toward thicker parts

THICKNESS VARIATION SYSTEM

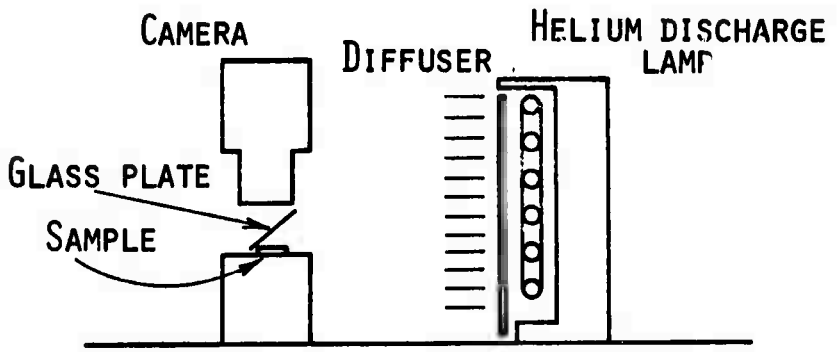

Figure 2a

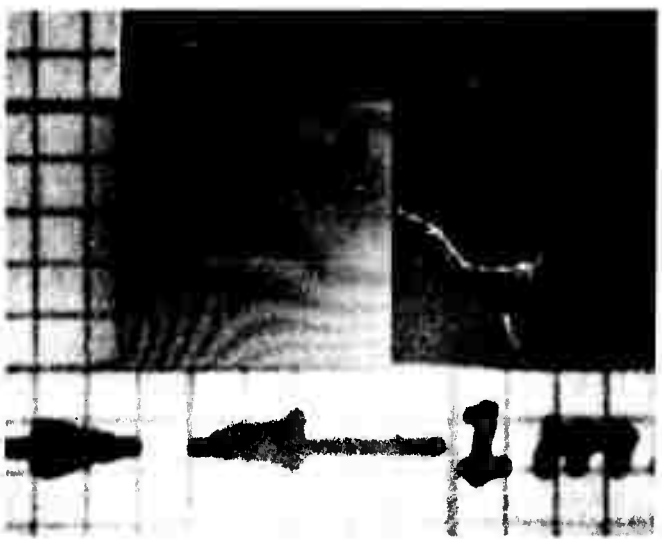

Figure 2b

Figure 2. Thickness Variation System

of the film. This can be seen as follows: The optical path difference between the light reflected from the front surface and that reflected from the film-substrate interface is given by Δ (OP) = 2nh cos θ' where θ' is the angle between the normal to the film and the propagation direction of the light internal to the film.(Ref. 6) As the sample is rotated away from the perpendicular, θ' increases from zero and the optical path difference at the spot of thickness h decreases. However the original dark band will move to a point at which Δ (OP) is the same as it originally was at the spot of thickness h, i.e. it must move in the direction of increasing h.

The combination of variable wavelength interferometry, monochromatic light photography, and visual inspection as a function of angle under the monochromatic light therefore provides us with complete thickness information at all points of the films. The characterization sheets provided with the samples supplied under the contract indicate thickness at two spots on the thickness map in order to establish the direction of thickness variation.

VII. Defect Detection and Location

Defects in a magnetic bubble film which impede the motion of bubble domains, at the very least will reduce device operating margins and in the worst case may render the film useless for device operation. Detection and location of such defects thus becomes an important phase of quality control, both in order to minimize damage at every stage of sample processing and for the selection of device quality areas.

Shumate (Ref. 7) has outlined a technique for the measurement which we have found convenient and, with some experience, quite sensitive. It involves the application of an alternating magnetic field normal to the film, of sufficient amplitude and frequency to cause appreciable domain motion when viewed in a polarizing microscope. Regions in which domains are still pinned at defects will be decorated by non-moving walls. The technique requires a judicious choice of field amplitude, since a large amplitude will tear domains away from weak pinning sites and those sites will go undetected. In practice the minimum amplitude which causes the blurred condition serves very well to delineate strong defects or those with some spatial extent such as scratches and clusters of point defects. For weaker point defects it is often necessary to go to lower amplitudes and look for points at which the domain pattern tends not to move or to move in a "snap-action" fashion. Both of these approaches are used in generating the defect maps provided with the samples.

The equipment used for this measurement is shown in Fig. 3a. The sample is manually scanned at 200X by an operator who, upon observing

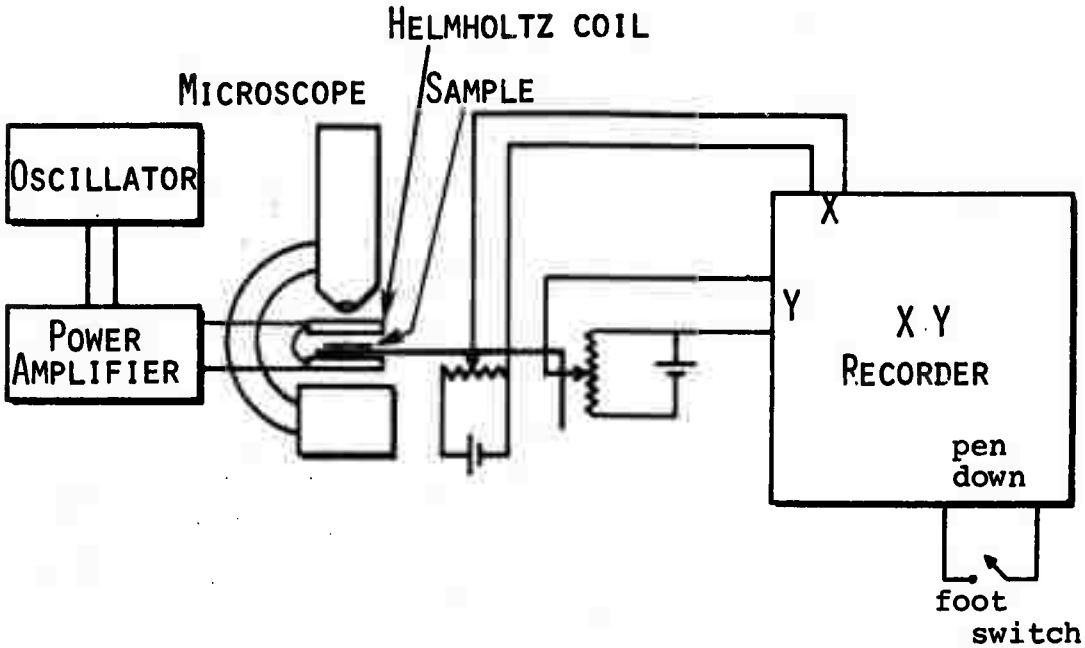

Figure 3a

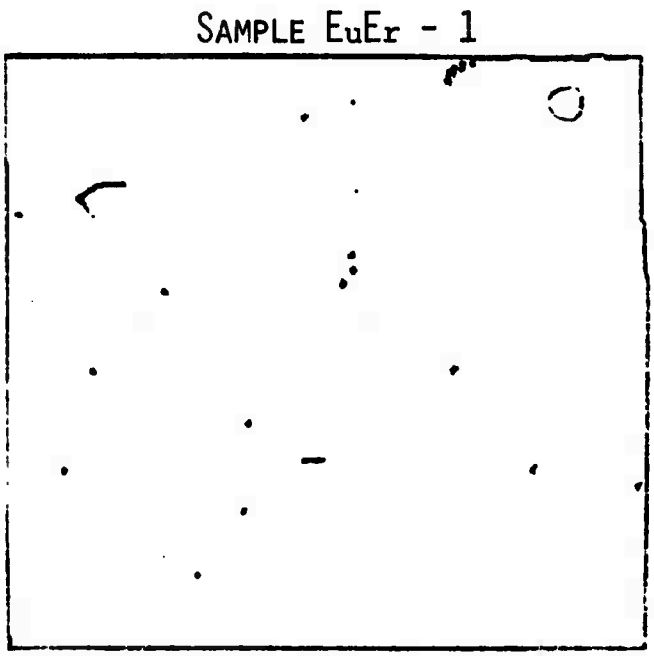

Figure 3b

Figure 3. Defect System

a region of domain wall pinning, centers it in the microscope field of view and presses the footswitch to drop the recorder pen and mark the map. The oscillator and power amplifier were used simply because they were already in place for other measurements. A variable voltage transformer operating directly off the 60 Hz line would be completely satisfactor for this measurement. A typical defect map of a 1 x 1 cm sample is reproduced in Fig. 3b.

It is difficult at this point to say whether all significant defects are being detected or whether some of those detected may, in fact, be too weak to cause problems. What is needed in this regard is a correlated study of defect strength from the above measurements and bubble propagation errors under a standard circuit mask. In the meantime every effort will be made in the materials growth area to eliminate all detectable defects.

VIII. Characteristic Length, ℓ, and Domain Dimensions

The characteristic length can be obtained directly from polarizing microscope measurements of domain sizes when coupled with either the theory of Thiele (Ref. 8) or that of Kooy and Enz (Ref. 9) for strip domains. The method associated with the Thiele paper requires the measurement of circular domain diameters at the stability limits. This method was quite satisfactory for the orthoferrites with their relatively large bubble diameters but becomes both inaccurate and tedious with the smaller bubbles in garnets. The method being used for this contract is the one developed at Monsanto and subsequently also reported by Fowlis and Copeland at the 17th. Magnetism and Magnetic Materials Conference (Ref. 10). It involves the measurement of the spatial period, P_0, of the strip domain pattern at zero applied field. This is generally accomplished using a calibrated microscope — graduated eyepiece combination but can also be recorded on film as in Fig. 4 . The various bubble diameters are also measured using this arrangement. In the determination of P_0 it is important to apply an AC bias field to the sample prior to measurement to avoid effects of coercivity. The AC field must be large enough to cause considerable wall motion, the amplitude being gradually reduced to zero after a useful straight domain pattern has been established. A pattern nearly always can be established which permits an average P_0 to be taken over approximately 20 periods thereby improving the accuracy of the determination a great deal. It is this property of the strip pattern which makes the technique preferable to that based upon bubble dimensions.

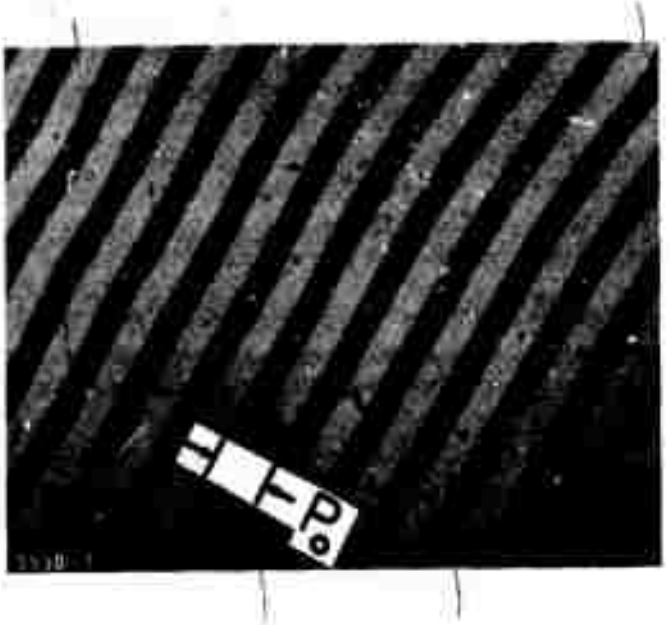

Figure 4. Typical Strip Domain Pattern at H = O Showing Domain Period, P_0. Magnification 500x

Once values of P_0 and film thickness, h, have been determined one must take recourse to theory to determine the characteristic length. The curve in Fig. 5 and the table I are based upon the strip domain theory of Kooy and Enz (Ref. 9) and agree fully with the recent calculations of Fowlis and Copeland (Ref. 10) and Cape and Lehman (Ref. 11). Care must be taken to measure P_0 at the same location at which h was determined in order to minimize error. The resulting uncertainty in ℓ for films of interest for devices should be no more than ± 10%.

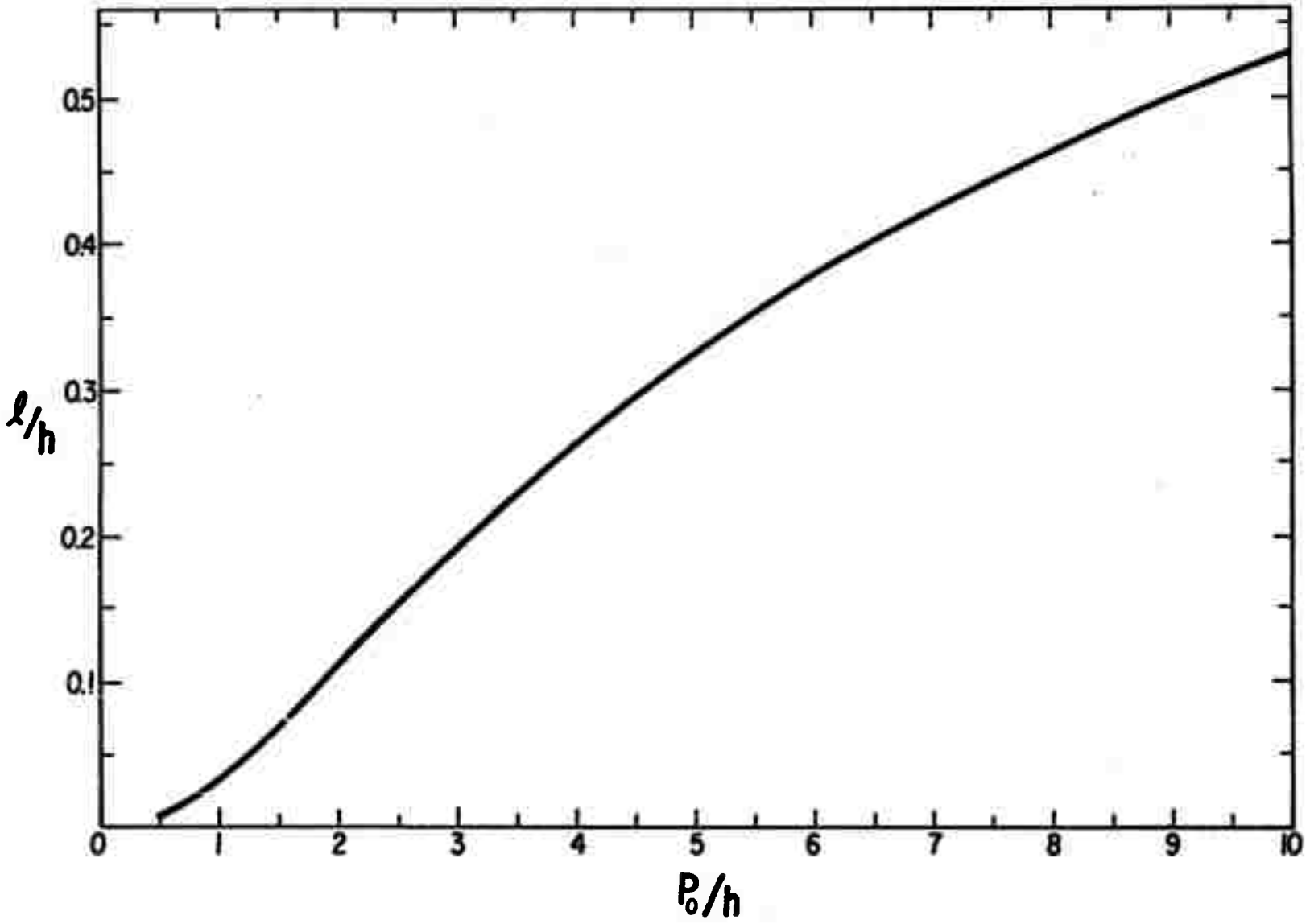

Figure 5. Characteristic Length Divided by Thickness vs. Strip Domain Period at H = O Divided by Thickness. After Kooy and Enz

TABLE I

Characteristic length divided by thickness vs. strip domain period divided by thickness. After Kooy and Enz

ℓ = Characteristic length

h = Film thickness

P_o = Spatial period of strip domains at zero applied field

P_o/h	ℓ/h
0.50	.0085
0.60	.0122
0.70	.0166
0.80	.0216
0.90	.0273
1.00	.0335
1.50	.0706
2.00	.1126
3.00	.1945
4.00	.2660
5.00	.3268
6.00	.3791
7.00	.4245
8.00	.4647
9.00	.5005
10.00	.5328
15.00	.6590
20.00	.7496
30.00	.8778

IX. Saturation Magnetization, $4\pi M_s$, and Magnetic Fields

The saturation magnetization generally appears in the Gaussian cgs system of units as $4\pi M_s$. For example, an ideal thick slab of uniaxial material would saturate in the easy direction at an applied field $H_s = 4\pi M_s$ in the limit of zero domain wall energy. The presence of a finite domain wall energy causes a curvature in the magnetization curve near saturation and leads to $H_s < 4\pi M_s$ but the combination $4\pi M_s$ remains the one most closely associated with other material parameters. For this reason sample characterization and this discussion are couched in terms of this combination.

Fowlis and Copeland (Ref. 10) have pointed out that $4\pi M_s$ can be determined from a knowledge of film thickness, h, zero field strip period, P_0, and the bubble collapse field, H_0. They have combined the Thiele theory (Ref. 8) for bubbles and the theory of Malek and Kambersky (Ref. 12) for strip domains. The resulting curve is shown in Fig. 6 while numerical values are given in Table II . While this method would appear to be less accurate than the hysteresis loop approach developed at Monsanto (Ref. 13), it offers the advantages of increased speed in data acquisition and analysis and permits simultaneous measurement of the stable range of bubble diameters and bias fields. A comparison of $4\pi M_s$ values obtained by this bubble collapse method and the hysteresis method indicates agreement to within approximately 4%. A comparison of the stable range of bubble diameters and bias fields with those predicted from the measured $4\pi M_s$ and the Thiele theory, shows a considerable variation, particularly in the

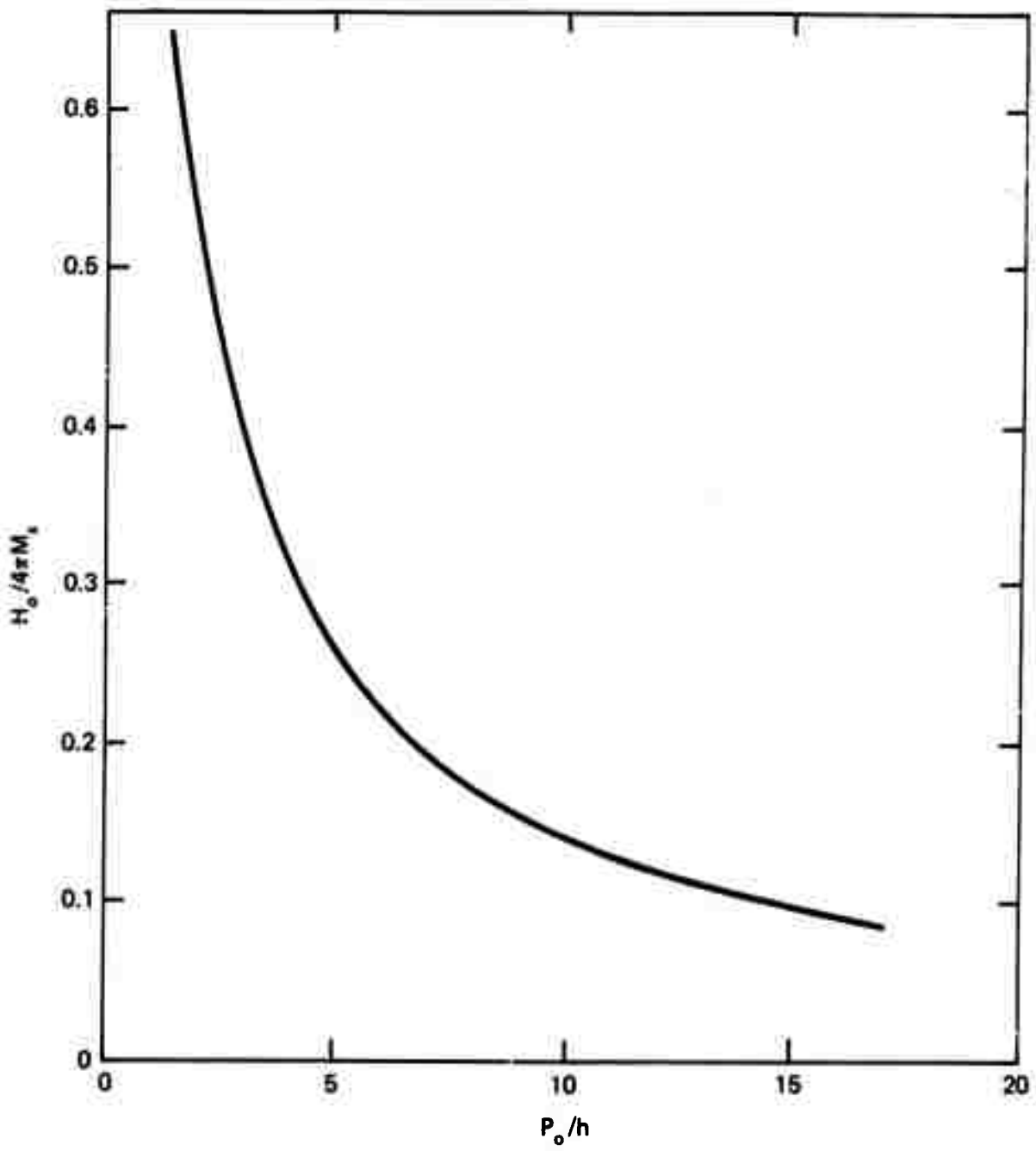

Figure 6. Bubble Collapse Field, H_0, Divided by $4\pi M_s$ vs. Strip Domain Period, P_0, at H = O Divided by Thickness, h. After Fowlis and Copeland

Table II

Bubble collapse field, H_0, divided by $4\pi M_s$ vs. strip domain period, P_0, at H = O divided by thickness, h. After Fowlis and Copeland.

P_0/h	$H_0/4\pi M_s$
1.50	0.608
2.00	0.518
2.50	0.447
3.00	0.393
3.50	0.349
4.00	0.314
4.50	0.285
5.00	0.261
5.50	0.240
6.00	0.223
6.50	0.208
7.00	0.194
7.50	0.182
8.00	0.172
8.50	0.163
9.00	0.155
9.50	0.147
10.00	0.140
10.50	0.134
11.00	0.128
11.50	0.123
12.00	0.118
12.50	0.113
13.00	0.110
13.50	0.106
14.00	0.102
14.50	0.099
15.00	0.095

bubble-to-strip diameter. An in-house study to determine which of these two methods yields the more reliable value for collapse and strip to bubble transition diameters is currently being carried out. If it proves possible to predict these stability limits at least as well as they can be measured (which seems likely in view of the limited accuracy of the bubble diameter measurement) then we will be in a position simultaneously to increase accuracy and to reduce data acquisition time.

The apparatus for measurement of collapse field consists simply of a polarizing microscope equipped with light source and bias coil, each with their respective power supplies. Fields are calculated from the measured current in the coil and a prior in-situ field vs. current calibration using an accurate Hall probe. The strip domain pattern is cut up with a fine iron wire tip prior to mounting in the microscope and the sample is indexed to the same spot at which h and ℓ have been determined. Care is taken when measuring H_0 that bubble interaction is negligible by selecting bubbles for observation which are at least 20 diameters apart. The uncertainty in H_0 is approximately $\pm 5\%$ which, when combined with the $\pm 4\%$ uncertainty in h, yields a probable error of $\pm 7\%$ in $4 \pi M_s$. Because of the hysteresis in the strip to bubble transition, it is felt that this field is in doubt to within $\pm 7\%$.

X. Anisotropy Field - H_A

The anisotropy field — that in-plane magnetic field required to force the magnetization vector to lie in the plane — enters into both the stability of bubble domains and their dynamics. In bubble materials H_A must be greater than $4\pi M_s$ for bubble domains to be stable (Ref. 8) . In order to avoid bubble to strip instabilities in a device being driven by a rotating field it is necessary to have H_A several times this lower stability limit, say $H_A \gtrsim 2\ (4\pi M_s)$. On the other hand the mobility of a domain is inversely proportional to $H_A^{1/2}$ (Ref. 14) as is the width of the domain wall. (Ref. 15). As this width decreases the strength of interaction with defects localized on a similar scale becomes greater, leading to an increase in coercivity and defect pinning. Thus a large anisotropy detracts from the dynamic capabilities of a bubble film while some minimum anisotropy is a necessity. The desirable range appears to be $2 \lesssim H_A/4\pi M_s \lesssim 8$.

A magneto-optical technique is being used at Monsanto for the measurement of H_A. The apparatus is shown in Fig. 7a . A large field, H_{dc}, is generated by an electromagnet and applied essentially in the plane of the film sample. Provision is made for minor rotation of the sample with respect to H_{dc}. An alternating field of amplitude 50 Oe or less, H_{ac}, is applied normal to the film by means of a Helmholtz coil (not shown). The laser beam, passing through the polarizer, sample, and analyzer, yields information regarding the average Faraday rotation in the sample. The Si detector responds to the total laser light transmitted of

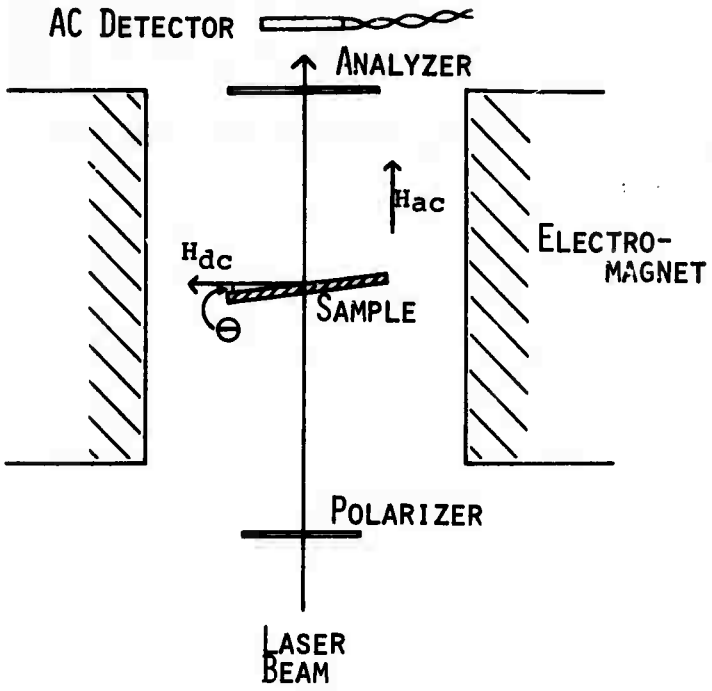

Figure 7a

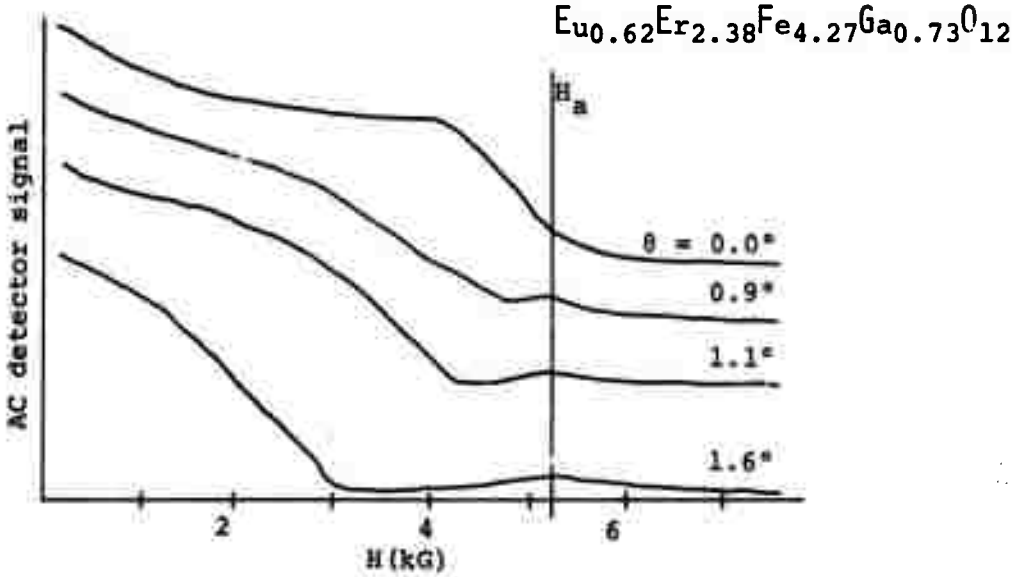

Figure 7b

Figure 7. Anisotropy System

which the AC component in synchronism with the alternating field is of interest. This is amplified by a lock-in amplifier referenced to the Helmoholtz coil frequency and the output plotted vs. the applied H_{dc} on an X-Y recorder.

Typical results from this system are shown in Fig. 7b . The several records have been vertically displaced for clarity. The signal at large H_{dc} is zero in all cases. At low values of H_{dc} the detected signal is due to domain wall motion. This signal goes to zero at a field which is strongly dependent upon the angle the sample makes with respect to H_{dc}. Zero signal occurs as a result of saturation of M along the easy axis when the component of H_{dc} in the easy direction reaches the saturating field. When the field is accurately in the plane of the film both domain types remain until the field H_A is reached and the signal remains large until that point, as shown for $\theta = 0.0$ in the Figure. For angles other than zero the sample saturates in one direction before M is pulled into the plane and the signal therefore drops at lower H_{dc}. In low coercivity samples it is often possible to observe a peak in the signal at fields just below this drop. This is a result of the wall susceptibility peak (or, equivalently, the steeper slope of the M vs. H magnetization curve) in this field range. After saturation a signal persists, however, and peaks at approximately H_A. This is a result of a spin susceptibility in which, crudely speaking, the spins seek to avoid the hard direction but can be switched from one side of this direction to the other. (Ref. 16). When H_{dc} becomes greater than H_A this signal decreases once again. The actual position of this peak is a function of both

the amplitude of H_{ac} and the component of H_{dc} normal to the film, being shifted to lower fields by increases in either of these. However, these effects are not large and the technique used here, in which θ is varied, can reasonably be expected to be accurate to within 10%.

XI. Coercivity - H_c

The coercivity is the field in excess of the equilibrium value required to cause a domain wall to move, i.e. one half of the hysteresis loop (M vs H) width. As such it represents an energy dissipation mechanism to be held to a practical minimum. It is well known that in most magnetic materials the hysteresis loops for small field excursions are not ideal parallelograms in which no change in M occurs until the major hysteresis loop is intersected. Rather, the minor loops continue to exhibit decreasing slope near H = O as the extent of the excursions is reduced. The magnetic garnets are rather well behaved in this respect but such effects do make the coercivity a somewhat nebulous parameter. The technique outlined below and used in the present contract is a reproducible approach to this measurement which appears to be gaining acceptance as the standard method (Refs. 7 and 17).

The Faraday effect in the magnetic film is utilized in a standard polarizing microscope arrangement. As in the anisotropy measurement, an alternating field is applied normal to the film plane and the light modulation caused by domain wall motion is synchronously detected using the apparatus of Fig. 8a . The resulting signal is plotted versus alternating field amplitude up to a maximum of approximately 7 Oe. If the hysteresis curves followed the ideal parallelograms referred to above, the modulation signal would fall to zero at an alternating field amplitude of H_c and there would be no modulation for smaller amplitudes. Such is not the case, as Fig. 8b shows. However a linear portion of the modulation

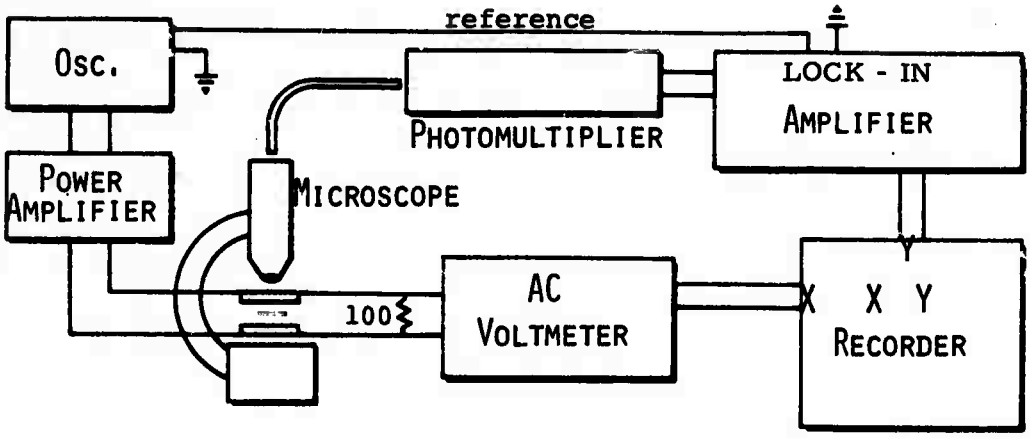

Figure 8a

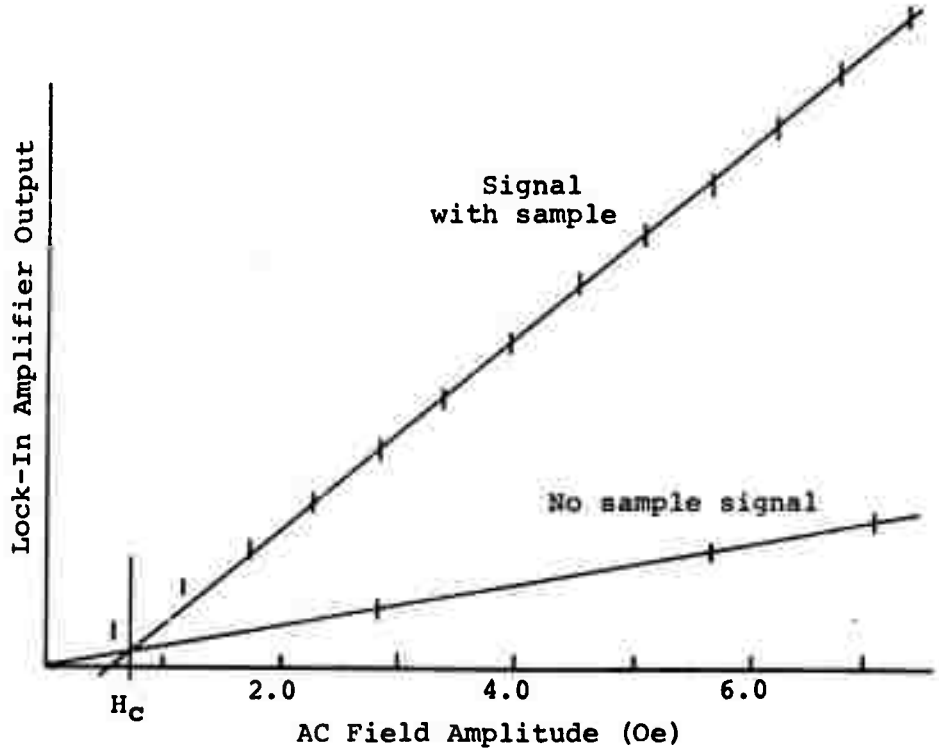

Figure 8b

Figure 8. Coercivity System

versus field amplitude curve does exist for larger amplitudes. This linear section, when extrapolated to zero modulation, serves to define a coercivity value which is, to a first approximation at least, free of the peculiarities which develop at very small field amplitudes. In Fig. 8b the short vertical lines are the data points obtained by setting the recorder pen down at fixed amplitude for a time greater than 10 time constants of the lock-in amplifier filter circuit.

Referring again to the apparatus of Fig. 8a it should be pointed out that, in this case and in that of the mobility measurement to be considered next, white light (including a great deal of infrared) is used to illuminate the sample. If silicon or an S-1 photomultiplier surface were used as detector, very little modulation would be observed because of the small Faraday rotation in the infrared (Ref. 18). Short wavelength pass filters can be used to improve this situation but the 6199 photomultiplier tube with its detection cutoff near 0.62 micron wavelength solves the problem admirably. Of course, any other tube with cutoff in this range would serve as well.

One other experimental point deserves comment here. All of the microscope optics tested to date exhibit a Faraday effect themselves. That is, there is a modulation signal present even in the absence of a sample. This may be as large as the signal from the sample in high magnetization samples and is presumably due to magnetic additions to the glasses used in fine microscope optics. Several things have been done to insure that the coercivity values quoted are valid and characteristic of the sample under

test. First, it has been determined that, within experimental uncertainty (± 0.05 Oe) the microscope optics signal is proportional to field amplitude and does not contribute a structure to the curve which would be interpreted as a coercivity. Second, the signal arising from the optics alone (at similar transmitted intensity) has generally been separately measured and used as the baseline as in Fig. 8b. Third, and most important, similar measurements carried out in a system which did not employ a microscope have yielded results for H_c which agree with the microscope results to within approximately 10%. This system, which uses a He-Ne laser beam and silicon detector, as in the anisotropy measurement, shows no such magneto-optical effect and provides a "clean" system for the determination of H_c. Unfortunately it was developed too late to process all samples in the first delivery. The comparative results lend credence to the values quoted, however. When all of the aforementioned matters are considered a reasonable estimate of the probable error in H_c is ± 20%.

XII. Domain Wall Mobility, μ_w

The domain wall mobility is defined in terms of the domain wall velocity, V_w, and in terms of the excess applied field over that which just causes the wall to move, H_{excess}, as

$$\mu_w = \frac{V_w}{H_{excess}} \ cm/_{sec - Oe}.$$

It is related to the mobility of a closed wall cylindrical domain by $\mu_d = 1/2\ \mu_w$ (Ref. 8) and, in conjunction with the maximum obtainable drive field will determine data rates in magnetic bubble devices. Several techniques have been proposed for the measurement of this quantity (Ref. 19 through 22). After experimentation with several of these, we have concluded that the optical detection of domain walls moving in response to a fast rise-time field pulse as proposed by Seitchik, Doyle, and Goldberg (Ref. 21) represents the most reliable method for garnet materials of modest mobility ($\mu_w \lesssim 50$ cm/sec/Oe). They show that the damped motion of the domain walls is governed by a time constant τ given by $\tau = (x_0/H_0)\mu_w^{-1}$

where x_0/H_0 is the domain wall displacement per unit applied field. This quantity can be calculated from P_0 and the initial slope of the magnetization curve, or, if $4\pi M_s$, P_0, and h are known, the initial magnetization slope can be found from Fig. 9 (Ref. 13). In the low field region in which only domain width changes occur a favored strip will grow in width by 0.1 P_0 for a change in M of 0.2 M_s. Thus an individual wall moves 0.05 P_0 in that interval and $x_0/H_0 = 0.05\ P_0/H\ (0.2\ M_s)$, where $H\ (0.2\ M_s)$ is the applied field at which $M = 0.2\ M_s$. This latter approach has been adopted as the standard procedure at Monsanto. Thus a measurement

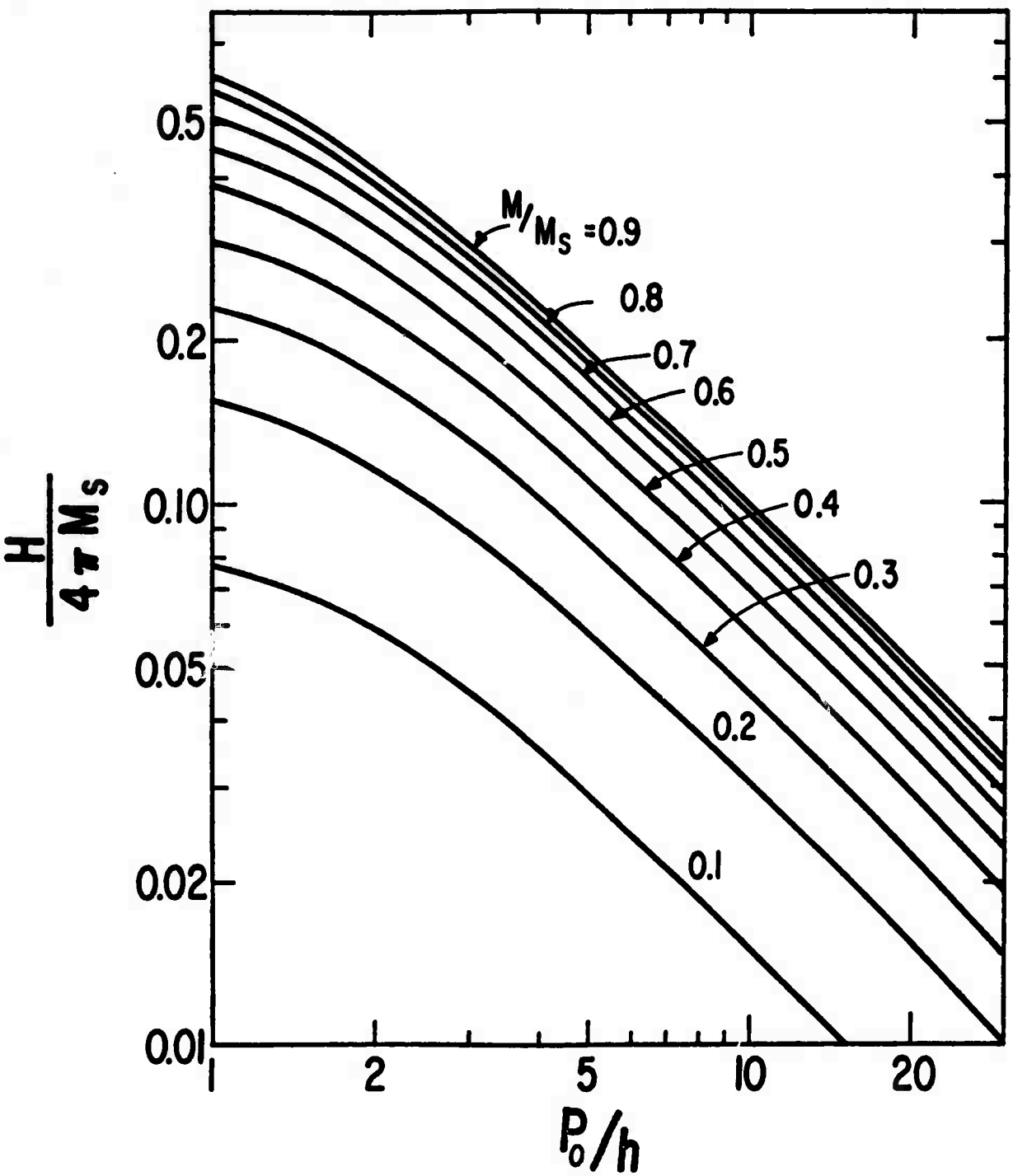

Figure 9. The Applied Field H Necessary to Achieve Various Magnetization Ratios M/M_s for Samples Exhibiting Zero Field Strip Domain Period P_0. Note the normalizations of the axes.

of the domain wall relaxation time τ and knowledge of the initial magnetization curve slope serve to determine the wall mobility as

$$\mu_w = (x_0/H_0)\,\tau^{-1}$$

The system used for the mobility measurement is shown in Fig. 10a The heart of the system is an oscilloscope with sampling plug-in unit which acts as a box-car integrator. As the domain walls move under the influence of the pulsed field, they modulate the optical Faraday effect. A photomultiplier detects the modulated light, and serves as the signal source for the sampling plug-in unit. The slow sweep generator, which is simply an operational amplifier integrating a small voltage, permits the sampled interval to be swept very slowly while the RC combination on the sampling unit output averages the resulting signal with a 3.5 sec time constant. The coil which generates the field pulse consists of 20 turns with an average diameter of 1.3mm. In the circuit shown, the pulse rise time is approximately 15 n sec. Pulse length is typically 5 μ sec and repetition rate 2KHz. Pulse amplitude is held below that which causes bubble generation or domain rearrangement to occur, typically 120 Oe in the EuEr compounds. No dependence of domain wall relaxation time on pulse amplitude was detected in these materials but for the garnets, generally, such an effect probably does exist (Ref. 23).

Typical results from this system are shown in Fig. 10b . The wall response is detected with a signal to noise ratio of approximately ten. When the normalized approach to the new equilibrium value is plotted against time elapsed after the pulse onset, Fig. 10c results. The reproducibility of

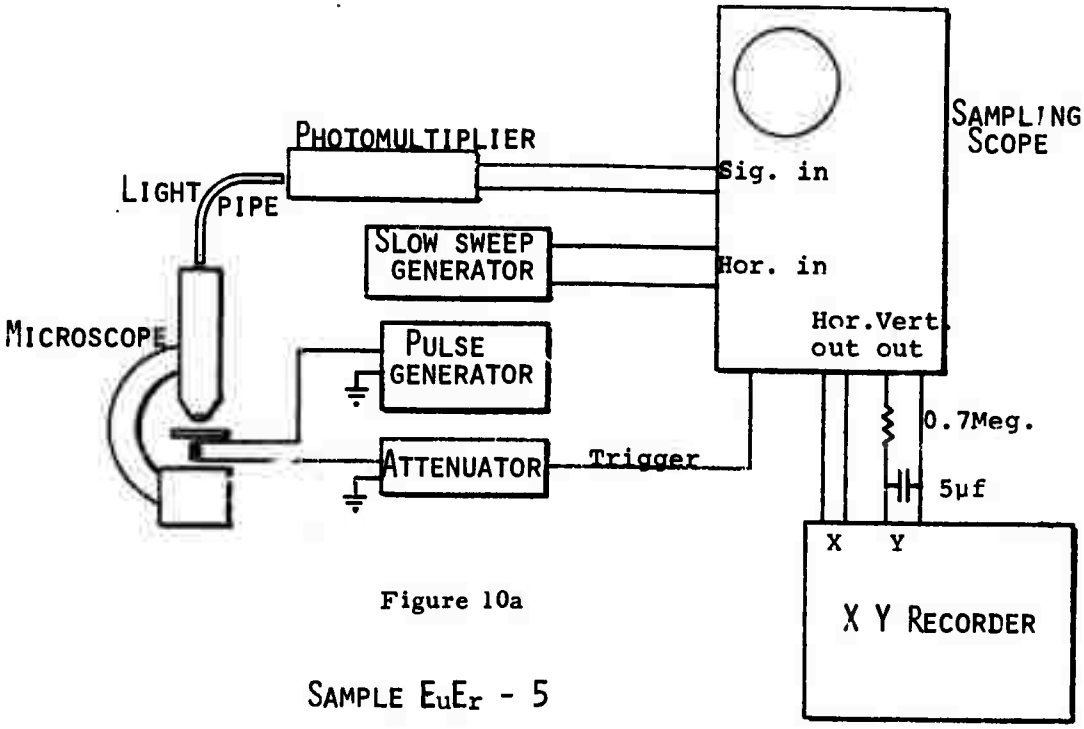

Figure 10a

SAMPLE E_uE_r - 5

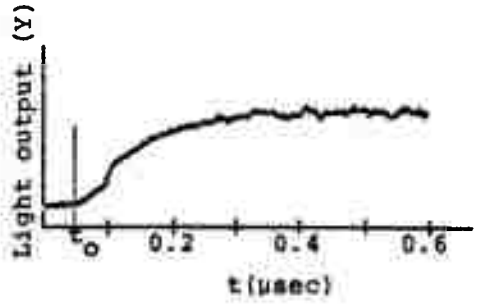

Figure 10b

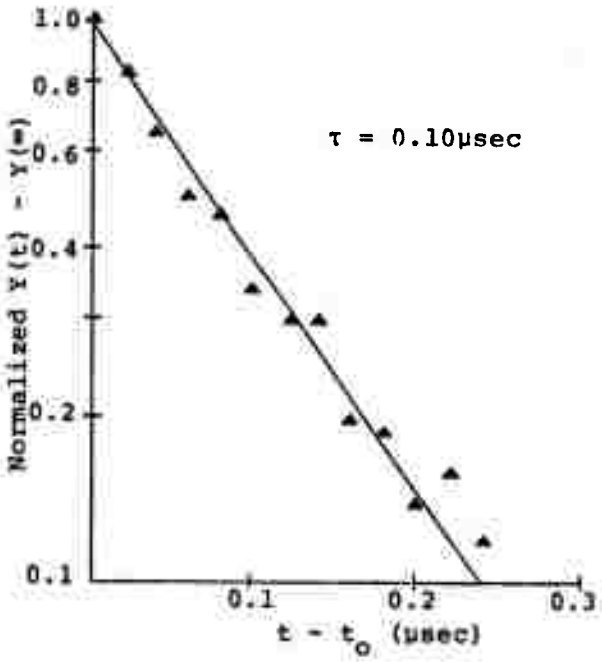

Figure 10c

Figure 10. Mobility System

this domain wall relaxation time measurement is approximately ± 15%. Because useful signal to noise ratios are difficult to obtain in the EuEr garnets at pulse amplitudes below approximately 40 Oe we have estimated the accuracy of the resulting mobility values to be ± 25%.

For higher mobility garnets, the present system may have to be modified to obtain a faster pulse rise time. Mobility measurements are being made with two other techniques, bubble collapse and bubble translation in an attempt to find the best technique for high performance garnets.

XIII. Neel Temperature, T_N

The Neel temperature in a uniaxial ferrimagnetic bubble garnet is the temperature at which the transition from ferrimagnetic to paramagnetic behavior occurs. The significance of this temperature lies in the fact that it decreases monotonically with Ga^{+3} substitution for tetrahedral Fe^{+3} in the pure iron garnet. When correlated with compositional data (obtained from electron microprobe, e.g.), measured values of T_N can be used routinely to determine the Ga^{+3} content of garnet films. T_N measurements taken at several points on the film yield information about the compositional homogeneity of the layer. If the gallium concentration varies by as much as one percent, the corresponding change in Neel temperature can be detected. This technique is more sensitive to gallium variation and the corresponding variation in tetrahedral iron than is electron microprobe, however it is very insensitive to changes in the rare earth metal ions.

The Neel temperature is being measured optically as shown in Fig. 11a by a technique suggested by Mee (Ref. 24) and more recently by Kurtzig (Ref. 25). A 150 Hz AC magnetic field of constant amplitude is applied to the sample which rests on a sapphire plate inside a Leitz heating stage. The domain walls move under the influence of this AC field, and modulate the optical Faraday effect. The light modulation is amplified by a photomultiplier and then synchronously detected by a lock-in amplifier. The DC signal from the amplifier, which is proportional to the domain wall susceptibility, is fed to an X-Y recorder whose X-axis is driven by a calibrated

chromel-alumel thermocouple imbedded in the heating stage. An example of the type of data obtained from this measurement is given in Fig. 11b. The Faraday susceptibility drops sharply to zero at the Neel temperature allowing a measurement precision of ±1°K to obtain.

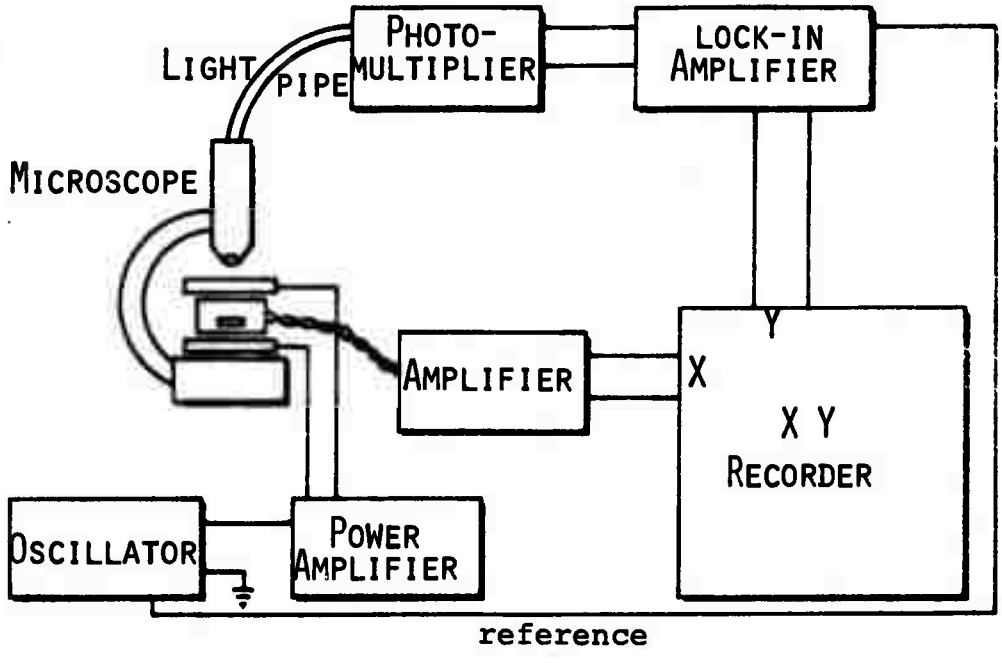

Figure 11a

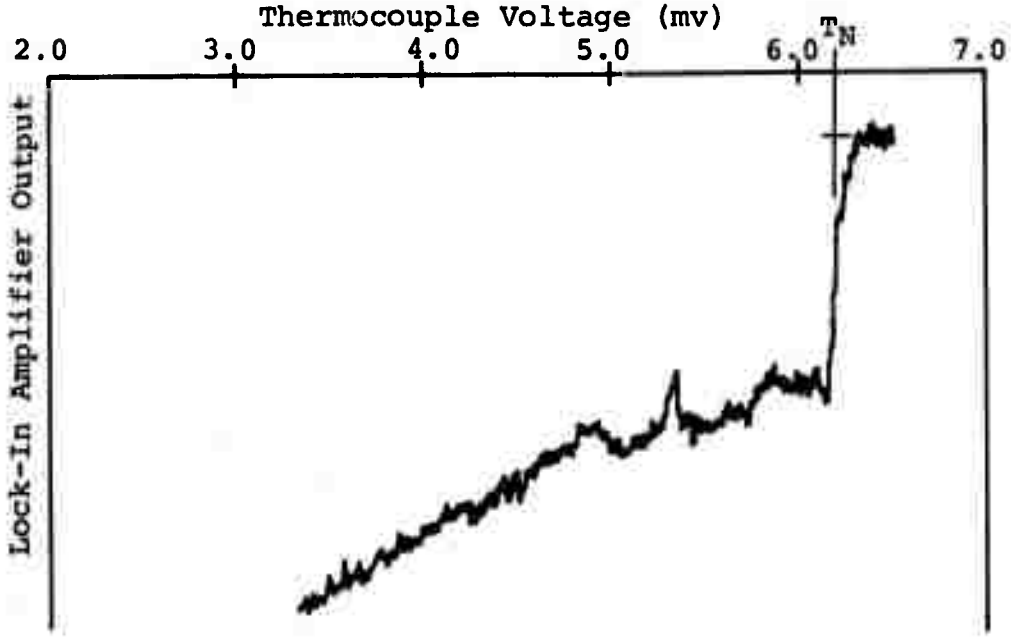

Figure 11b

Figure 11. Neel Temperature System

XIV. Conclusion

The characterization techniques used at Monsanto for magnetic bubble materials are summarized in Table III. Where appropriate the probable error in each result has also been indicated. In concluding this report a few specific comments are in order.

Several of the techniques employed would seem to have evolved already to the point where only minor modifications resulting in greater speed of data acquisition and processing are to be expected. These include the methods employed for lattice parameter, thickness and its variation, and Neel temperature. A second group which may be avoidable in the future because of correlated studies going on in several laboratories at present includes composition determination by electron microprobe and the measurement of the various bubble diameters and fields.

The characteristic length and saturation magnetization measurement techniques described herein seem to be well on their way to acceptance although the need for greater accuracy may force refinements later. The method for defect detection and location is more tedious than one would like. At present there is no more convenient alternative applicable to the garnets but the development of one is much to be desired. Finally, the techniques for measurement of anisotropy field, coercivity, and mobility are too new and the alternatives too numerous to be able to say, with any certainty, what the standard approach will be. In particular the mobility technique described herein is appropriate only for materials with rather modest mobility. Once the domain wall relaxation time approaches the

rise time of the field pulse (15 n sec in our case but perhaps as short as 3 n sec with special care) the technique ceases to be accurate. A number of other techniques can then be used but these generally have disadvantages in terms of accuracy, convenience and/or complexity. It is definitely too early to say which, if any, of the existing techniques will be adopted as standard for this critical measurement. Much work remains in the development of techniques for the evaluation of bubble materials, however the progress in this area thus far has been very rapid and will undoubtedly continue apace. Within reasonable limitations of expense and complexity the techniques outlined in this report are felt to be the best available at this time.

Table III

Magnetic Bubble Materials Characterization Summary

Property	Technique	Probable Error Limits
*Composition	Electron microprobe analysis and Neel temperature	± 3%
*Lattice parameter	X-ray diffraction	± 0.0001Å
**Substrate defects	Polarized and phase interference microscopy	
Thickness	Reflectivity in wavelength range 0.6 to 1.0 microns	± 4%
Thickness variation	Monochromatic light photograph	± 4%
Defects	Microscopic examination in alternating field	
Defect location	X-Y map of sample	± 0.1mm
ℓ - characteristic length	H = O strip domain width and sample thickness using theory	± 10%
$4\pi M_s$	ℓ, bubble collapse field, and thickness using theory	± 7%
H_A - anisotropy field	Crossed DC and AC fields with Faraday effect detection	± 10%
H_c - coercivity	Extrapolation of Faraday effect signal to $H_{AC} = O$	± 20%
μ_w - wall mobility	Dynamic wall motion (bubble collapse or translation as needed)	± 25%
T_N - Neel temperature	Hot stage with field modulation and photomultiplier readout	± 1°K
Bubble diameters	Calibrated microscope eyepieces	± .5 μ
Bias fields	Fixed field coils calibrated by Hall probes	± 2%

* Applied to both substrates and films ** Applies to substrates only.
All other properties apply to films only.

APPENDIX I

Equipment List

Composition

Cambridge MKII scanning electron probe microanalyses employing one X-ray detection channel with capability of measurement for elements of atomic number 13 and higher

Substrate Defect Identification

Microscopes - Leitz Ortholux

- Reichert Phase Contrast

Lattice Parameter

X-Ray - General Electric XRD-5 Diffractometer with attachments for precise lattice measurement from -60 to + 1500°C

Thickness

Lamp - Westinghouse 250Q/CL250 watt quartz-iodine bulb.

Chopper and power supply - American Time Products 42C at 200 Hz

Monochromator - Heath EU-700 with 590 lines/in. grating

Light pipes - Corning Glass No. 5013 - 6ft. lengths

Si Solar Cells - International Rectifier S0505E5PL

Lock-In amplifiers - Signal channel - Princeton Applied Research HR-8 with Type A preamp preamplifier

Reference channel - Composite system including AMF preamplifier No. LA 460F and the following Burr Brown units: 3144/15, 3020/15, 9859/15, 3195/15, 3056/01, and 4032/12C

Divider - Burr Brown 106A

Recorder - Bausch and Lomb VOM-6

Thickness Variation

Camera - Polaroid MP-3 system with 35mm focal length lens.

Helium Lamp and Diffuser - Lapmaster monochromatic light No. CP-1

Defect Detection and Mapping

Oscillator - 1 channel, Hewlett Packard Model 203A

Power Amplifier - Kepco BOP36-5M

Microscope - Leitz Ortholux

Rectilinear potentiometers - Bourns Model 116

X-Y recorder - Moseley 7030AM

Characteristic Length

Microscope - Leitz Ortholux

$4 \pi M_s$

Microscope - Leitz Ortholux

Power supply - Hewlett Packard 6824A

Anisotropy field

Oscillator - Hewlett Packard 200CDR

Power amplifier - Bogen MO-100A

Laser - Spectra Physics Model 132

Detector - International Rectifier S 1010 E 6 PL

Electromagnet - Varian V-4007 with V-2200A Power Supply and Fieldial.

Lock-In Amplifier - Princeton Applied Research Model 120

X - Y Recorder - Moseley 7035 A

Coercivity

Oscillator - Hewlett Packard 200 CDR

Power amplifier - Hewlett Packard 6824 A

Microscope - Leitz Ortholux

Photomultiplier - RCA 6199 with Fluke 412B Power Supply

Lock-In Amplifier - Princeton Applied Research Model 120

AC Voltmeter - Hewlett Packard 400 E

X - Y Recorder - Moseley 7035 A

Mobility

Rulse Generator - Hewlett Packard 214 A

Photomultiplier - RCA 6199 with Fluke 412 B Power Supply

Sweep Generator - Burr Brown 3010 Operational Amplifier

Sampling oscilloscope - Tektronix 585 A with 1S1 Plug-in

X-Y Recorder - Moseley 7030 AM

Neel Temperature

Oscillator - Hewlett Packard 200 CDR

Power Amplifier - Hewlett Packard 6824 A

Microscope - Leitz Ortholux

Hot stage - Leitz 350°C

Thermocouple amplifier - Keithley 155

Photomultiplier - RCA 6199 with Fluke 412 B Power Supply

Lock-In Amplifier - Princeton Applied Research Model 120

X-Y Recorder - Moseley 7035 A

References Cited

1. P. J. Besser, J. E. Mee, P. E. Elkins and D. M. Heinz, Mat. Res. Bull. 6, 1141 (1971).

2. E. D. Pierron and J. B. McNeely, "Advances in X-ray Analysis", Plenum Press, Inc., N. Y., 1969, Vol. 12, p. 343.

3. See, for example, John Strong, Concepts of Classical Optics (W. H. Freeman, San Francisco, Cal., 1958) p. 154.

4. op. cit. p. 530

5. B. J. Roman, R. R. Spiwak, and S. A. Baron, "Epitaxial Garnet Thickness Determinations from Near Infrared Interferometry", Bell Laboratories Memorandum of May 25, 1971.

6. See, for example, F. A. Jenkins and H. E. White, Fundamentals of Optics, 2nd Ed. (McGraw Hill, New York, N. Y. 1950) p. 255.

7. P. W. Shumate, Jr. IEEE Trans. Magn., vol MAG-7, p. 586.

8. A. A. Thiele, Journ. Appl. Phys. 41, 1139 (1970)

9. C. Kooy and U. Enz, Philips Res. Repts. 15, 7 (1960).

10. D. C. Fowlis and J. A. Copeland, "Rapid Method for Determining the Magnetization and Intrinsic Length of Magnetic Bubble Domain Materials" paper 4F-7 presented at the 17th Conference on Magnetism and Magnetic Materials, Chicago, Ill. 1971.

11. J. A. Cape and G. W. Lehman, Journ. Appl. Phys. 42, 5732 (1971).

12. Z. Malek and V. Kambersky, Czech. J. Phys. 21, 416 (1958).

13. R. W. Shaw, D. E. Hill, R. M. Sandfort, and J. W. Moody, Bull Am. Phys. Soc. Ser. II, 17, 108 (1972)

14. L. Landau and E. Lifshitz, Phys. Z. Soviet Union 8, 153 (1935). See also J. A. Cape, "Dynamics of Bubble Domains", to be published.

15. S. Chikazumi, Physics of Magnetism, (Wiley, N. Y., 1964) p. 191

16. E. J. Torok, R. A. White, A. J. Hunt, and H. N. Oredson Journ. Appl. Phys. 33, 3037 (1962).

17. P. P. Luff, private communication.

18. C. D. Mee, Contemp. Phys. 8, 385 (1967).

19. F. C. Rossol, J. Appl. Phys. 40, 1082 (1969).

20. A. H. Bobeck, I. Danylchuk, J. P. Remeika, L. G. Van Uitert, and E. M. Walters, "Dynamic Properties of Bubble Domains" presented at 1970 Int. Conf. Ferrites, Kyoto, Japan. Further analysis in H. Callen and R. M. Josephs, J. Appl. Phys. 42, 1977 (1971).

21. J. A. Seitchik, W. D. Doyle, and G. K. Goldberg, J. Appl. Phys. 42, 1272 (1972).

22. J. A. Copeland and R. P. Spiwak, IEEE Trans. Magn. vol. MAG-7, 748 (1971).

23. B. E. Argyle, J. C. Slonczewski, and A. F. Mayados "Domain Wall Motion in Rare Earth Substituted Ga: YIG Epitaxial Films". paper 3E-10 presented at the 17th. Conference on Magnetism and Magnetic Materials, Chicago, Ill., 1971.

24. C. D. Mee, IBM Journal 11, 468, 1967.

25. A. J. Kurtzig, R. C. LeCraw, A. H. Bobeck, E. M. Walters, R. Wolfe, H. J. Levinstein, and S. J. Licht, "Correlation of Domain Wall Mobility with Gallium Concentration in Bubble Garnets," paper 3E-11 presented at the 17th Conference on Magnetism and Magnetic Materials, Chicago, Ill. 1971.